

Article

One-Step Fabrication of Inverted Pyramid Textured Silicon Wafers via Silver-Assisted Chemical Etching Combing with Synergism of Polyvinylpyrrolidone (PVP)

Yuchen Liu , Kousuo Dong, Linsheng Bian and Zisheng Guan *

College of Materials Science & Engineering, Nanjing Tech University, 30 South PuZhu Road, Nanjing 211816, China; 201861103001@njtech.edu.cn (Y.L.); 201961103069@njtech.edu.cn (K.D.); 201961203164@njtech.edu.cn (L.B.)

* Correspondence: zsguan@njtech.edu.cn or zishengguan@163.com; Tel.: +86-138-1393-2186

Abstract: Inverted pyramid-texturing of silicon surface has been proven to have great application potential in silicon solar cells. In this paper, we utilized Ag-assisted chemical etching (Ag-ACE) technology combing with polyvinylpyrrolidone (PVP) to fabricate an inverted pyramid textured Si surface. We call it Ag@PVP-ACE. The effect of different experimental parameters on etching results was observed. We show that the microstructure of the Si surface exhibited two states as the concentration of NH_4HF_2 and PVP concentration changed: polishing and inverted pyramid texturing. Meanwhile, we found inverted pyramids easier to form at the high temperature and low H_2O_2 concentration of the etching system. Consequently, compared to inverted pyramid structures fabricated by nanostructure rebuilding (NSR) technology and Ag@PVP-ACE, we consider that Ag@PVP-ACE technology could become a viable strategy for fabricating inverted pyramid textured Si wafers in Si solar cells production.

Keywords: inverted pyramid; metal-assisted chemical etching; synergism; textured single crystalline silicon wafers



Citation: Liu, Y.; Dong, K.; Bian, L.; Guan, Z. One-Step Fabrication of Inverted Pyramid Textured Silicon Wafers via Silver-Assisted Chemical Etching Combing with Synergism of Polyvinylpyrrolidone (PVP). *Crystals* **2021**, *11*, 459. <https://doi.org/10.3390/cryst11050459>

Academic Editor: Wen Lei

Received: 2 April 2021

Accepted: 19 April 2021

Published: 21 April 2021

Publisher's Note: MDPI stays neutral with regard to jurisdictional claims in published maps and institutional affiliations.



Copyright: © 2021 by the authors. Licensee MDPI, Basel, Switzerland. This article is an open access article distributed under the terms and conditions of the Creative Commons Attribution (CC BY) license (<https://creativecommons.org/licenses/by/4.0/>).

1. Introduction

Light-trapping structure fabrication is an essential step in Si solar cell production [1–3]. The significant reduction of surface reflectivity enhances light absorption and thus improves the conversion efficiency of solar cells [4]. As reported in single crystalline silicon (sc-Si) solar cell with the conventional upright pyramid, normally, the average reflectivity is limited to 10–14% [5,6], it was difficult to further reduce the surface reflectivity of upright pyramid textured Si. Thus, the inverted pyramid has attracted the attention of many researchers due to its controllable low surface reflectivity and secondary reflection of light in the structure [7–9].

As a simple wet chemical etching method to fabricate micro/nanostructure of Si surface. More attention has been paid to metal-assisted chemical etching (MACE) in recent years [10]. Various structures of Si prepared by MACE have presented application potentials in fields ranging from solar cells [2,11,12], Si photoelectrodes [13], chemical and biological sensing [14–17], thermoelectric transform [18,19], Li-ion batteries [20–22], semiconductor micro/nano devices [23–25] and more. MACE has been involved local coupling of redox reactions, catalytically generated electric fields caused by bipolar electrochemical reaction and autonomous movement aroused from self-electrophoresis of noble metal particles [26]. It is acknowledged that H_2O_2 is reduced faster around silver nanoparticles. The holes (h^+) are concentrated at the Si/Ag interface and injected from the metal into the silicon valence band [10,27]. The self-electrophoresis model reported by Peng and his coworkers was that the etching of the local Si layer around noble metal particles and the catalytic electric field further pushed the noble metal particles into the inner of Si wafers [28]. Ag [29,30] and Cu [31] are used as the most common catalysts

in MACE. However, other catalysts have been reported, such as Pt [32], Pd [33], Au [34], C [35], etc. The commonly used oxidants in MACE are H_2O_2 [36] and HNO_3 [37]. Other oxidants are rarely used, such as V_2O_5 [38].

It is worth mentioning that MACE is always used to fabricate the inverted pyramid structure of the Si surface [1,39]. The manufacturing process of an inverted pyramid can be divided into one-step and multistep methods. Du et al. utilized Cu particles to fabricate an inverted pyramid by a one-step method. They have reported that solution composition and concentration significantly affected the structure of Si surface, inverted pyramid, V-groove, hybrid structure, and upright pyramid were observed in the evolution of textured Si surface morphologies [40]. In addition, they considered that the anisotropic etching process, which resulted in the formation of an inverted pyramid, is mainly derived from noble metal particles that are easier to obtain electrons from {100} crystal planes than {111}. Thus, the difference of noble metal nanoparticle deposition density on different crystal planes resulted in the anisotropic characteristic of etching rate [40,41]. Nanostructure rebuilding (NSR) technology has been reported as a common multistep method to fabricate the inverted pyramid [5,8,42]. Deposited Ag particles accelerated the etching rate of the local Si layer to form nanopores, then utilized NSR treatment to fabricate the inverted pyramid via anisotropic etching [42,43].

In this paper, we fabricated the inverted pyramid of Si surface through Ag-assisted chemical etching technology combining with the synergism of polyvinylpyrrolidone (PVP), which we called Ag@PVP-ACE. As a safe and efficient etching agent, ammonium hydrogen difluoride (NH_4HF_2) was used to replace HF for rapidly etching SiO_2 [44] in our work. Koker et al. [45] confirmed that the etching rate of HF_2^- is about 15 times faster than HF via the photoelectrochemical method. In addition, polyvinylpyrrolidone (PVP) is a well-known surfactant and stabilizer [46] that has attracted attention to its structure-directing characteristics of controlling the length and diameter of noble metal particles [47]. The critical factors in achieving polishing or fabricating inverted pyramid in Ag@PVP-ACE process were revealed, and a systematic investigation was performed to confirm the parameters condition of fabricating inverted pyramids in Ag@PVP-ACE process. We compared the microstructure obtained by Ag@PVP-ACE and NSR technology and analyzed the difference. Furthermore, the difference in optical properties between the structure of upright, inverted pyramids is revealed.

2. Materials and Methods

2.1. Materials

Diamond-wire-sawn (DWS) (100)-oriented p-type Si wafers ($156.75 \times 156.75 \text{ mm}^2$, $180 \pm 10 \mu\text{m}$ thickness, the resistivity of $0.5\text{--}1.5 \Omega\cdot\text{cm}$) were employed in experiments, and all of above p-type silicon wafers were born-doped. Silver nitrate (AgNO_3 , AR), hydrogen peroxide (H_2O_2 , 30%, GR) were obtained from Sinopharm Chemical. High purity deionized water with a resistivity of $18.25 \text{ M}\Omega\cdot\text{cm}^{-1}$ was used in the experiment. Ammonium hydrogen fluoride (NH_4HF_2 , AR) was purchased from Nanjing Chemical Reagent Co., Ltd. (Nanjing, China). Aqueous ammonia ($\text{NH}_3\cdot\text{H}_2\text{O}$, 25%, AR) was purchased from Shanghai Ling Feng Chemical Reagent Co., Ltd. (Shanghai, China). Polyvinylpyrrolidone (PVP-K12/K30/K88-96, AR) was received from Shanghai Aladdin Biochemical Technology Co., Ltd. (Shanghai, China). All laboratory supplies were used as-received.

2.2. Experimental Method

A wet chemical etching aqueous solution containing AgNO_3 , H_2O_2 and NH_4HF_2 (Ag-ACE) along with the addition of polyvinylpyrrolidone (Ag@PVP-ACE) was used in our experiment. We explored the optimal conditions for fabricating inverted pyramid structure through a series of experiments with different parameters, as shown in Table 1.

Table 1. Experiment parameters used in Ag@PVP-ACE for fabricating inverted pyramid.

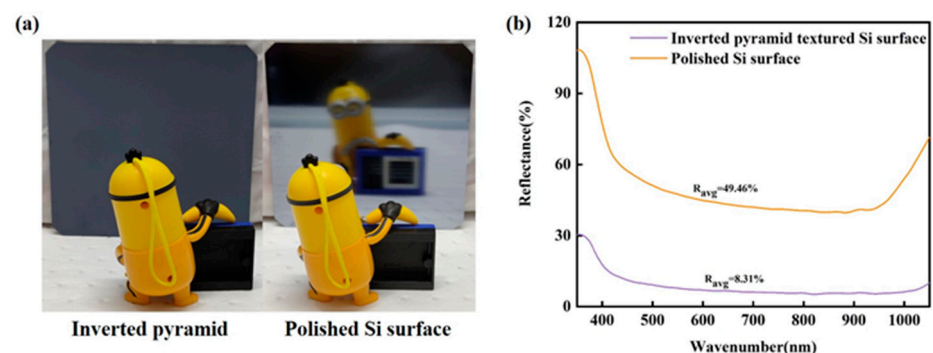
Experiment Parameters	Range
NH ₄ HF ₂	0.175–1.75 M
H ₂ O ₂	0.3–1.5 M
PVP	0.1–1.5 wt%
Temperature	45–75 °C

DWS Si wafers were immersed vertically into the Ag@PVP-ACE solution for fabricating inverted pyramid textured surface. Then etched Si wafers were immersed into deionized water for 2 min. Moreover, the textured Si wafers were rinsed in NH₃·H₂O (0.1 M) solution with H₂O₂ (0.1 M) for 3 min to remove residual Ag particles. Afterward, Si wafers were rinsed in pure water for 30 s and HF (0.1 M) solution for 1 min to clean the residual aqueous ammonia. Consequently, rinsing the silicon wafer repeatedly with deionized water and drying.

The surface and cross-sectional morphologies of Si wafers were observed by field-emission scanning electron microscopy (FESEM, Hitachi, 4800) and scanning electron microscopy (SEM, JEOL, JSM-IT200). The sample's reflectivity spectra in the wavelength range of 350–1050 nm were measured by UV-vis-NIR spectrophotometer (UV-3101PC, Japan, with an integrating sphere). The average reflectivity was calculated by measuring the reflectivity of nine areas evenly distributed on the surface of the Si wafer.

3. Results

As shown in Figure 1, etching results exhibited two completely different phenomena—fabrication of inverted pyramid or polishing. The object mirroring was completely invisible due to the existence of the inverted pyramid light-trapping structure on the Si surface; a clear object outline appeared on the polished Si surface (Figure 1a). Correspondingly, inverted pyramid textured prepared by Ag@PVP-ACE exhibited low reflectivity, the average reflectivity reached 8.31%, and the average reflectivity of Si surface polished by Ag@PVP-ACE reached 49.46%.

**Figure 1.** Photograph (a) and reflectance spectrum (b) of polished and etched samples in Ag@PVP-ACE.

3.1. Effect of PVP and NH₄HF₂ Concentration on Etching Results in Ag@PVP-MACE

The etching results were related to NH₄HF₂ and PVP concentration in Ag@PVP-ACE solution, as shown in Figure 2a. The inverted pyramid (Figure 2b–d) was normally produced at low PVP concentration and high NH₄HF₂ concentration. A polished Si surface (Figure 2e–g) appeared under high PVP concentration and low NH₄HF₂ concentration. In addition, the polymer molecular weight of PVP in the solution significantly affected the etching results. The addition of K12 and K30 to an aqueous Ag-ACE solution was more inclined to manufacture a polished Si surface. However, under some circumstances, the addition of K88-96 in Ag-ACE was easier to manufacture the inverted pyramid structure on the Si surface. Thus, we utilized K88-96 to complete the subsequent experiments.

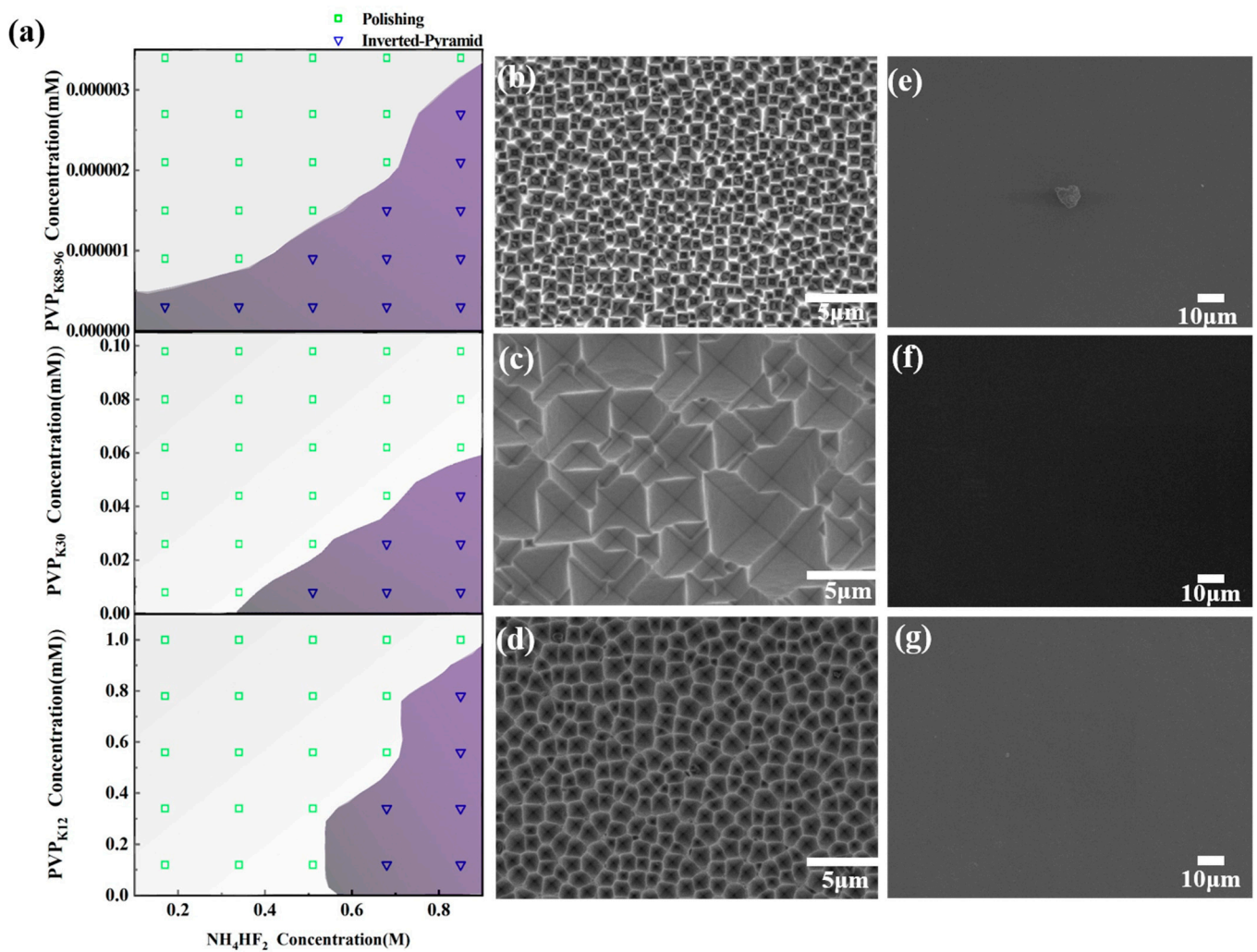


Figure 2. Dependence of the etching results (a) on NH_4HF_2 and PVP concentration and SEM images of inverted pyramid fabricated by Ag@PVP-ACE (b–d) and polished Si surface after treatment with Ag@PVP-ACE solution (e–g). The above samples were etched in mixed solution with 94 mM AgNO_3 and 0.9 M H_2O_2 for 20 min at 65 °C.

The transformation of the etching results was directly related to the absorption effect of PVP on Ag particles because PVP was more inclined to bind the {111} crystal plane of Ag particles [46,48]. The fabrication of inverted pyramids arose from the weak absorption effect of PVP when the PVP concentration was low. As PVP concentration increased, the adsorption effect of the PVP enhanced continuously, resulting in difficulty for single Ag particles to move directly into the inner of Si. Due to the steric hindrance of Ag@PVP , the vertical etching process of Ag@PVP-ACE became unapparent. Thus, the polishing process occurred. A high NH_4HF_2 concentration made it easier to generate the inverted pyramid structure, which was attributed to the transformation of etching behavior of Ag@PVP-ACE solution. A. M. Khort et al. observed that HF_2^- was different from F^- in etching mechanism, HF_2^- was conducive to the formation of porous silicon, but F^- was more inclined to occur plane-parallel etching [49]. With the increase of NH_4HF_2 concentration, the tendency of vertical etching that resulted from the amount of HF_2^- increase strengthened, which further weakened the effect of PVP. Therefore, a higher NH_4HF_2 concentration was more conducive to the fabrication of an inverted pyramid. At this moment, the NH_4HF_2 concentration played a leading role in the Ag@PVP-ACE process.

3.2. Effect of H₂O₂ Concentration on Etching Results in Ag@PVP-ACE

Figure 3 illustrates the dependence of samples surface average reflectivity on the concentration of H₂O₂ and NH₄HF₂. It can be clearly observed that as the concentration of NH₄HF₂ increased continuously, the surface reflectance first decreased and then increased. When the concentration of NH₄HF₂ was 0.175 M, the surface reflectivity etched by different H₂O₂ concentrations in solution was above 40%. When the concentration of NH₄HF₂ in the solution reached 0.35 M, the surface reflectivity reduced to 33% at low H₂O₂ concentration (0.3–0.9 M), while at high H₂O₂ concentration (1.2–1.5 M), the Si surface reflectance reduced to less than 20%. It is worth mentioning that etched Si surface average reflectivity increased as NH₄HF₂ concentration improved when the H₂O₂ concentration of the solution was 1.2–1.5 M. However, a similar situation did not appear when the H₂O₂ concentration was 0.3–0.9 M. The surface reflectivity did not change much as the NH₄HF₂ concentration increased to 1.05 M. Afterward, average reflectivity of the etched Si surface slowly raised as NH₄HF₂ concentration improved.

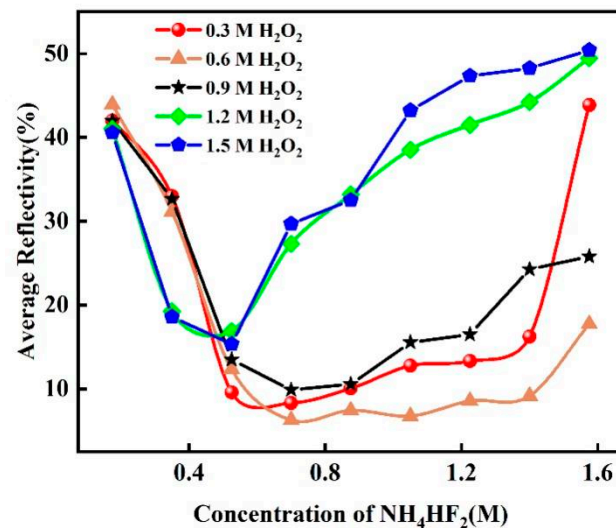


Figure 3. Dependence of samples surfaces average reflectivity on the concentration of H₂O₂ and NH₄HF₂ in mixed solution with 94 mM AgNO₃ and 9×10^{-7} M PVP. All experiments were performed at 65 °C for 20 min.

Figure 4 shows the corresponding SEM images of samples etched by Ag@PVP-ACE with different H₂O₂ concentrations under 0.175 M NH₄HF₂. When the H₂O₂ concentration was 0.3 M, some large-sized shallow square grooves appeared on the Si surface, and the overall morphology was relatively flat (Figure 4a). The surface morphology became flatter when the concentration of H₂O₂ was 0.6 M (Figure 4b). However, the difference was that the shallow round groove was generated when H₂O₂ concentration increased to 1.2–1.5 M (Figure 4c,d). The process of transforming square groove to round groove means that anisotropy of the etching process was weakened as NH₄HF₂ concentration increased.

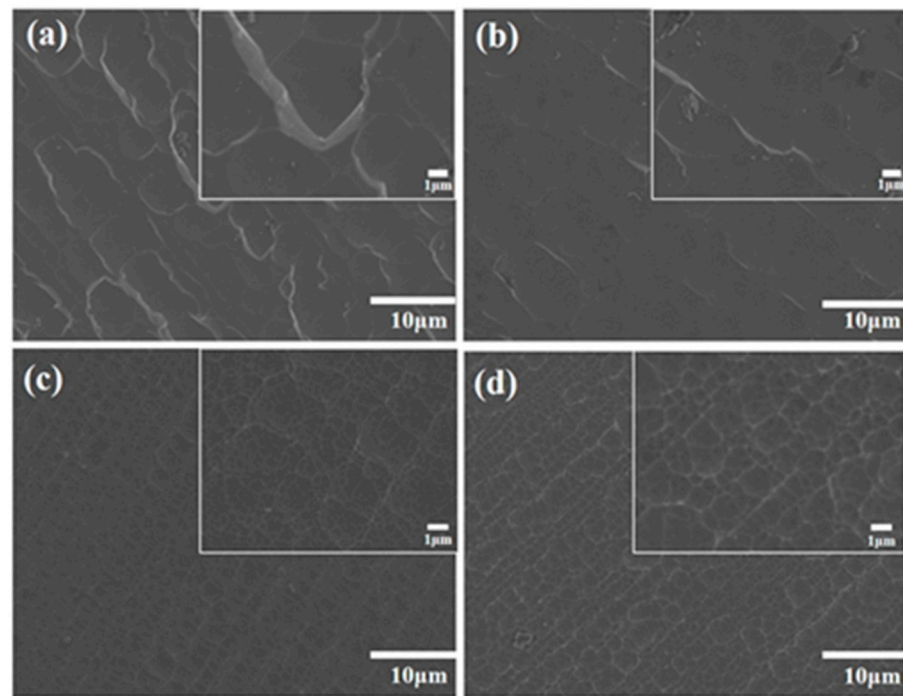


Figure 4. SEM images of the Si surface etched in 0.175 M NH_4HF_2 Ag@PVP-ACE solution with different H_2O_2 concentration: (a) 0.3 M; (b) 0.6 M; (c) 1.2 M; (d) 1.5 M. All above samples were etched at 65 °C for 20 min.

As for p-type Si, it was difficult to confine the holes under the Ag/Si contact interface. The holes would drift away from the p-type Si surface via the effect of the interface catalytic electric field (Figure 5a). Thus, the hole distribution density of different parts of the Si was obviously different. An anisotropy etching process of MACE occurred [27] (Figure 5b). With the increase of H_2O_2 concentration, ultra-high H_2O_2 concentration would inject additional holes into the Si valance band. The difference of holes distribution density reduced. As a result, anisotropic etching was weakened. By contrast, the isotropic etching process enhanced, the transformation of the square groove to round groove occurred via the etching behavior of Ag@PVP-ACE changes (Figure 5c).

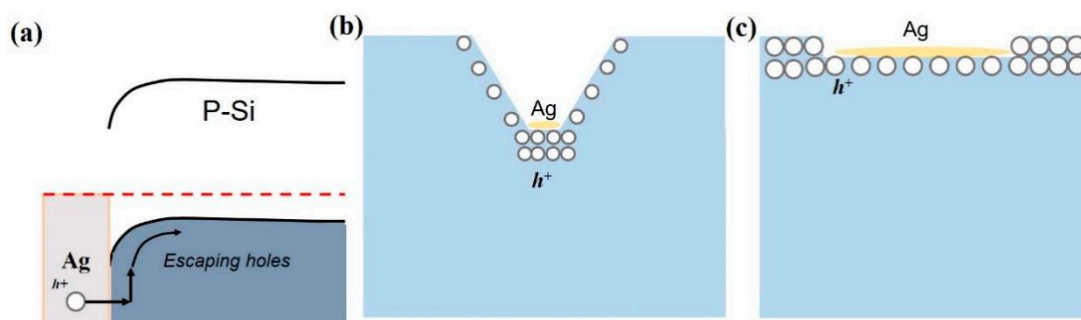


Figure 5. Schematic of Schottky barrier of Ag/Si contact interface (a) and transformation of etching behaviors by holes injection difference: (b) low H_2O_2 concentration; (c) high H_2O_2 concentration.

The samples treated in 0.875 M NH_4HF_2 -Ag@PVP-ACE with different H_2O_2 concentrations are shown in Figure 6. Large-scale inverted pyramid randomly distributed on the Si surface when H_2O_2 concentration was 0.3–0.6 M (Figure 6a,b), and inverted pyramid structure became shallow as H_2O_2 concentration increase to 1.2–1.5 M (Figure 6c,d). The above experimental results indicated that excessive H_2O_2 concentration did not apply to the formation of an inverted pyramid, whose average reflectivity was difficult to reduce

effectively to less than 10% (Figure 3). As mentioned before, the increase of NH_4HF_2 concentration accelerated the formation of pores. However, there was a certain balance between oxidation rate and etching rate. The appearance of a shallow inverted pyramid was caused by an intense oxidation process and low SiO_2 etching rate.

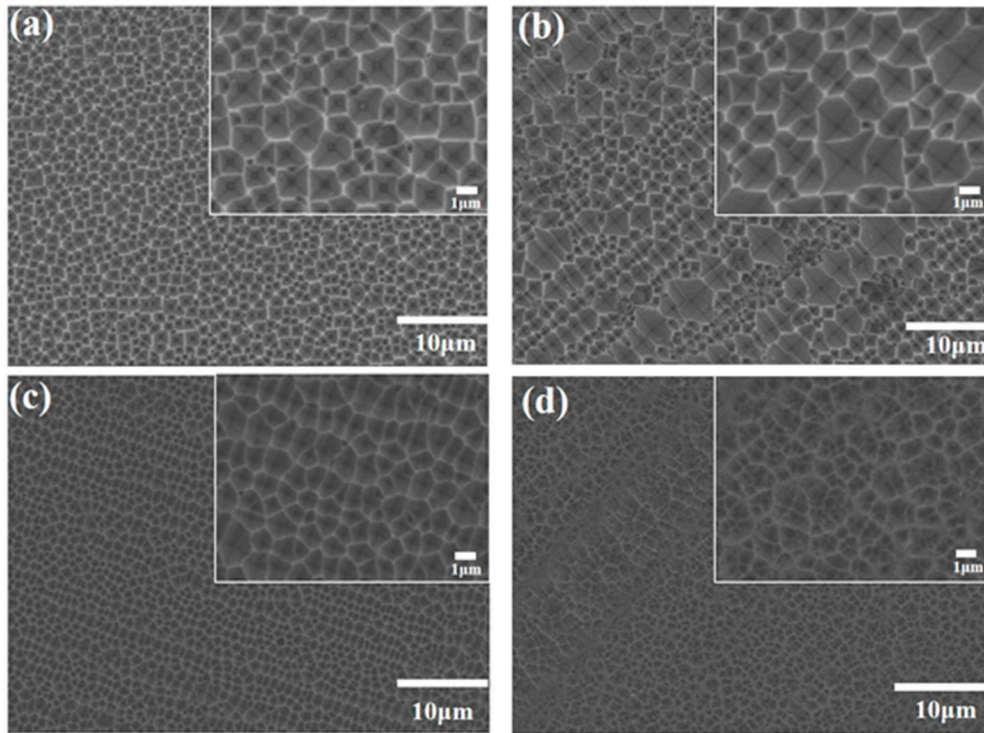


Figure 6. SEM image of the Si surface etched in 0.875 M NH_4HF_2 Ag@PVP-ACE solution with different H_2O_2 concentration: (a) 0.3 M; (b) 0.6 M; (c) 1.2 M; (d) 1.5 M. All above samples were etched at 65 °C for 20 min.

3.3. Effect of Temperature on Etching Results in Ag@PVP-ACE

Figure 7 shows the effect of etching temperature on the surface morphology of the DWS-Si wafers treated in Ag@PVP-ACE. The inverted pyramid structure fabricated at 45–55 °C was clearly shallow, and the four side edges of the inverted pyramid were blurred (Figure 7a,b). As the etching temperature increased to 65 °C, the depth of the inverted pyramid increased, and the four side edges were clearly distinguishable (Figure 7c–e). Results of reflectance spectrum were interrelated to surface morphology (Figure 7f), the reflectivity of Si wafers etched at 45–55 °C was significantly higher than the Si surface obtained by high-temperature (65–85 °C). It seems that NH_4HF_2 activity in the solution is positively related to temperature, but the oxidizing ability of H_2O_2 is rarely affected by the temperature. Under equal solution conditions, the etching process at low-temperature was dominated by H_2O_2 . It is acknowledged that there was an obvious difference in the thickness of the thermal oxide layer on different Si crystal planes [50]. It was difficult for the low reactivity of NH_4HF_2 to completely remove the oxide layer of each crystal plane, which resulted in the appearance of a shallow inverted pyramid. The high etching rate of NH_4HF_2 could effectively remove the oxide layer of different crystal planes with increasing etching temperature. Namely, the etching rate was faster than the oxidation rate, which resulted in the anisotropic etching behavior of Ag@PVP-ACE enhanced. Hence, it was easier to generate the inverted pyramid with a high aspect ratio at high-temperature.

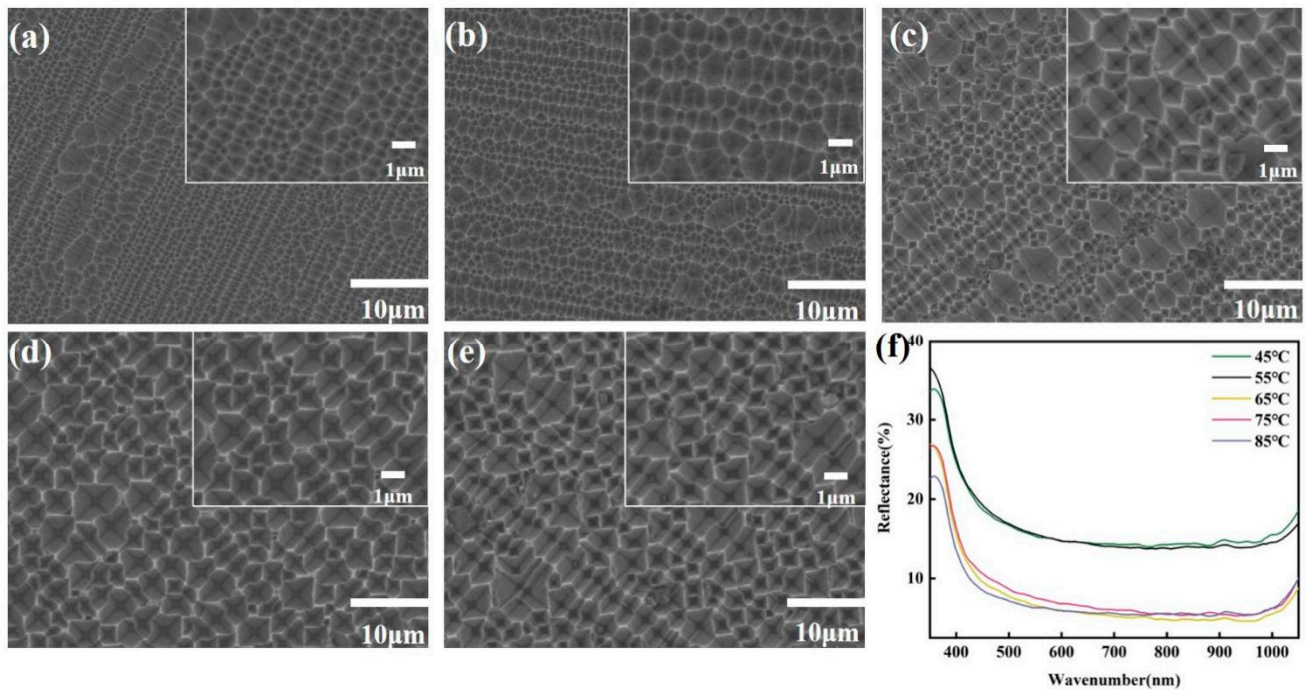


Figure 7. Effect of etching temperature on etched Si surface morphology: (a) 45 °C; (b) 55 °C; (c) 65 °C; (d) 75 °C; (e) 85 °C and corresponding reflectance spectrum (f).

3.4. Effect of Time on Etching Results in Ag@PVP-ACE

The effect of time on the etching results is shown in Figure 8. It is obvious that the average reflectivity of Si wafers first decreased and then increased with prolonging etching time. The reflectivity of samples etched for 10–30 min was lower than 10%. Combining with the above experiment results, we considered that 0.6 M H₂O₂ was most beneficial for the inverted pyramid texturing process. With the above parameter conditions at this moment, NH₄HF₂ concentration (Figure 3) and temperature changes (Figure 7f) had little effect on the surface reflectivity after etching.

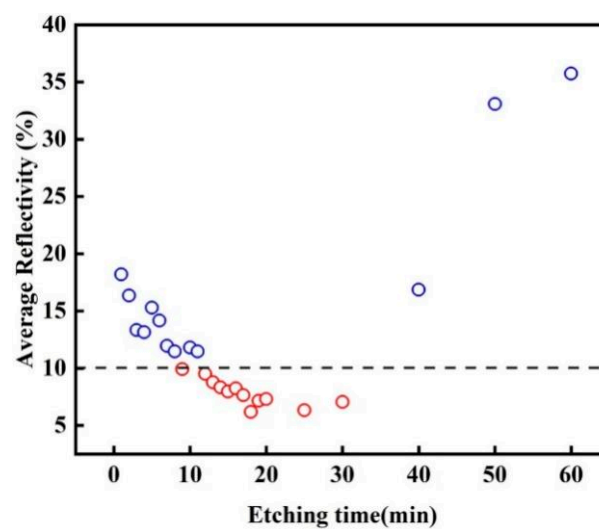


Figure 8. Effect of etching time on results in Ag@PVP-ACE with 0.875 M NH₄HF₂, 94 mM AgNO₃ and 0.6 M H₂O₂. All samples were etched for 6–60 min at 65 °C.

4. Discussion

4.1. Comparative Analysis of NSR and Ag@PVP-ACE Technology for Fabricating Inverted Pyramid

We compared the inverted pyramid formation process of NSR treatment and Ag@PVP-ACE, as shown in Figure 9. As for the fabrication process of inverted pyramids in Ag@PVP-ACE, first, shallow inverted pyramid grooves appeared locally on the Si surface via anisotropic etching (Figure 9a), then dense inverted pyramid grooves distributed randomly on the Si surface (Figure 9b). As the etching process continued, large-sized inverted pyramid holes emerged (Figure 9c). Completely different from Ag@PVP-ACE was that many nanopores needed to be manufactured on the Si surface first, before NSR treatment (Figure 9d). During the NSR treatment, nanopores expanded (Figure 9e) and then inverted pyramid formed via anisotropic etching (Figure 9f). The above results are consistent with the phenomenon in Figure 8. What was completely different from NSR technology was that the surface reflectivity decreased from high to low at the initial etching stage (0–15 min) of Ag@PVP-ACE. However, the reflectivity of Si treated by NSR technology would first decrease and then increase. Due to the difference in etching behavior in NSR and Ag@PVP-ACE, the appearance of many nanopores resulted in low surface reflectivity at the beginning of the texturing process. Afterward, the formation of a large-sized inverted pyramid structure via anisotropic etching increased the surface reflectivity in the NSR process (Figure 9g). As for the Ag@PVP-ACE technology, nanopores were replaced by shallow inverted pyramid square grooves on the Si surface. The relatively smooth surface resulted in higher surface reflectivity at the beginning of the etching process. Subsequently, the depth and distribution density of many inverted pyramid structures whose increased, and the inverted pyramid grooves transformed to inverted pyramid pores, which resulted in a gradual decrease in reflectivity (Figure 9h).

As shown in Figure 10, the inverted pyramid after NSR treatment was regular and square holes (Figure 10a). However, the uneven distribution of inverted pyramid structure led to a significant difference in structure size. The size of the structure was mainly distributed in 0.2–0.6 μm and 1–1.2 μm (Figure 10c). The inverted pyramid prepared by Ag@PVP-ACE exhibited uniform and relatively flat textured Si surface (Figure 10b), the size of structure mainly distributes in 1.5–2.0 μm , and the distribution characteristics were more similar to the normal distribution (Figure 10d).

The significant difference in the size distribution of the inverted pyramid structure treated by NSR technology can be attributed to the inconsistent depth of the nanopores, as shown in Figure 11a. It is difficult to regulate the depth of nanopores in the MACE process. Thus, under the same etching rate, nanopores with smaller depth would preferentially form an inverted pyramid, while nanopores with the larger depth needed to remove more Si layer from the hole walls to form regular inverted pyramid (Figure 11b), inverted pyramids with different depths appeared on the surface of Si wafers (Figure 11c).

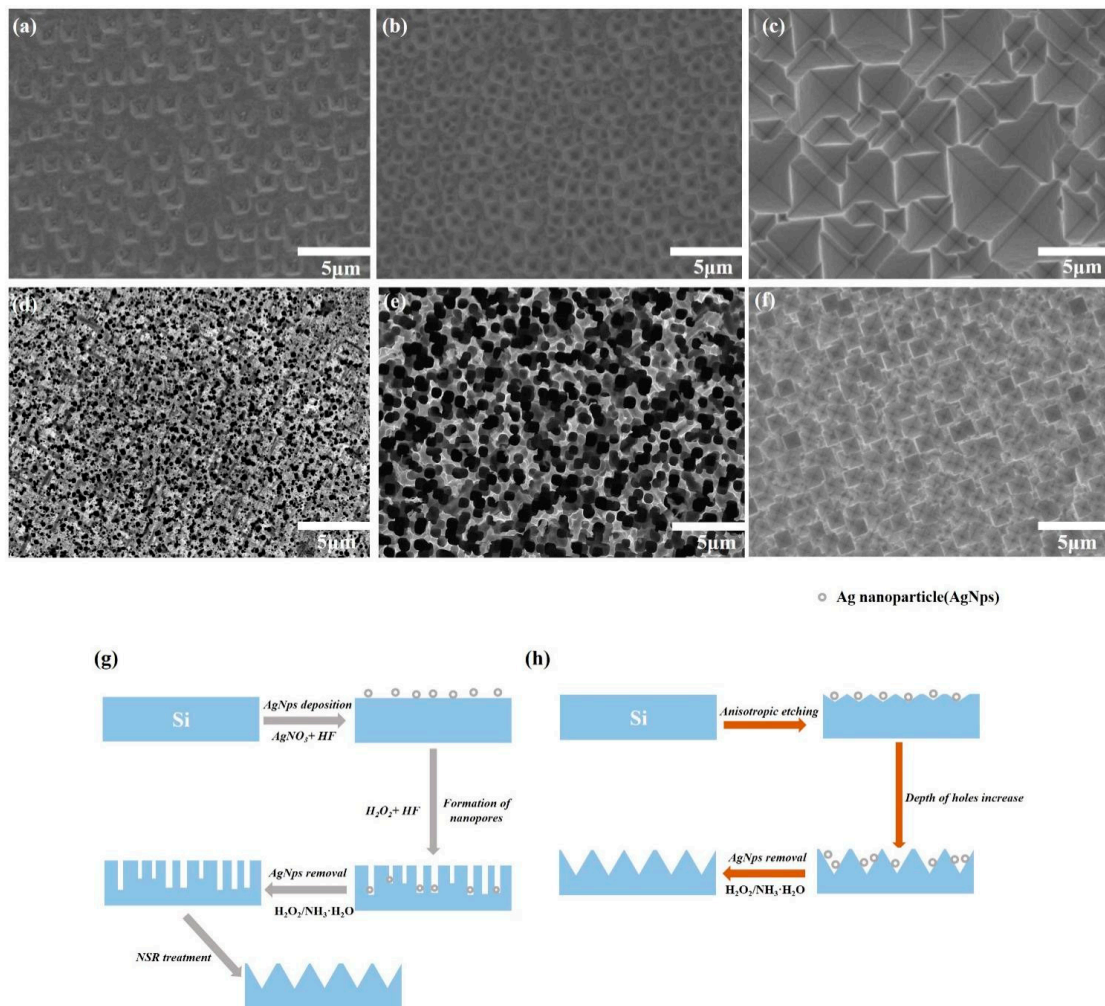


Figure 9. SEM images of inverted pyramid formation process via Ag@PVP-ACE (a–c), nanopore formation and NSR treatment (d–f) and corresponding schematic diagram of inverted pyramid fabrication process by NSR treatment technology (g) and Ag@PVP-ACE (h).

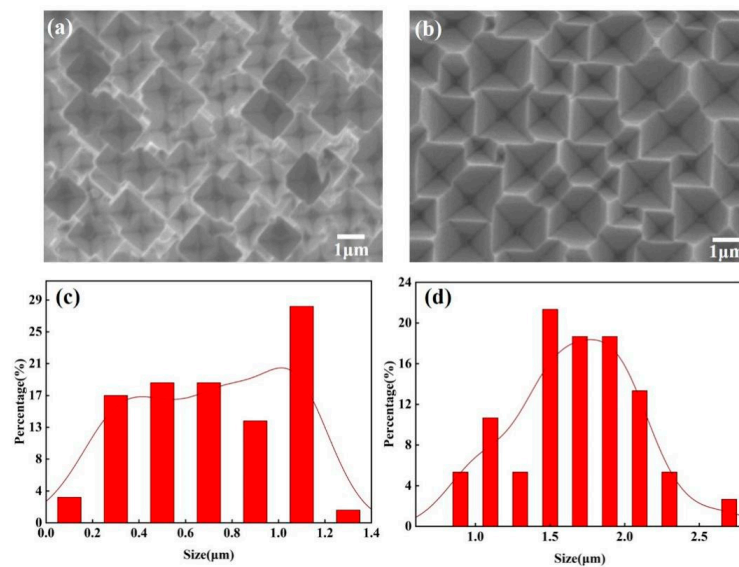


Figure 10. SEM image and results of sample structure size: (a,c) NSR technology processed inverted pyramid structure; (b,d) Ag@PVP-ACE one-step textured inverted pyramid structure.

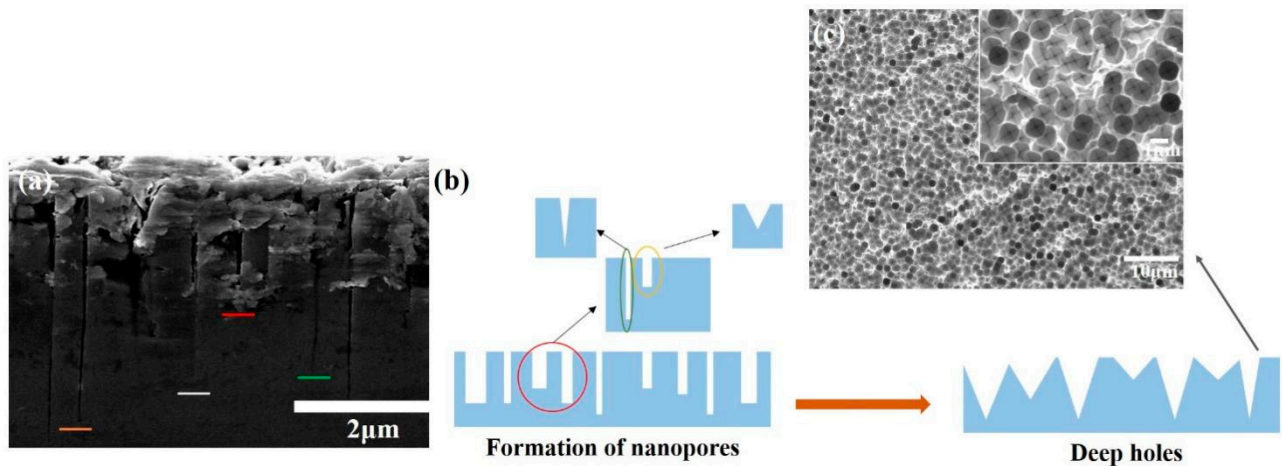


Figure 11. Cross-sectional SEM images of nanopores (a) and schematic diagram of nanopores treated by NSR process (b,c).

During the process of transforming deep nanopores into a complete inverted pyramid structure, the inverted pyramid structure formed by shallow pores was easily damaged due to further etching, which made the etching process difficult to control. The etching process needed to be controlled more precisely to obtain the ideal inverted pyramid structure (Figure 12a) in the NSR process, prolonged etching process led to the destruction of a large number of an inverted pyramid, and the inverted pyramid was replaced by an upright pyramid on the Si surface (Figure 12b). Because no nanopores were fabricated on the Si surface at the initial Ag@PVP-ACE stage, the inverted pyramids were almost formed on a similar plane. Thus, the inverted pyramid fabricated in the Ag@PVP-ACE process was more uniform in size and distribution (Figure 12c). Furthermore, increasing etching time would only cause the inverted pyramid to shallower, but the shape remained unchanged (Figure 12d).

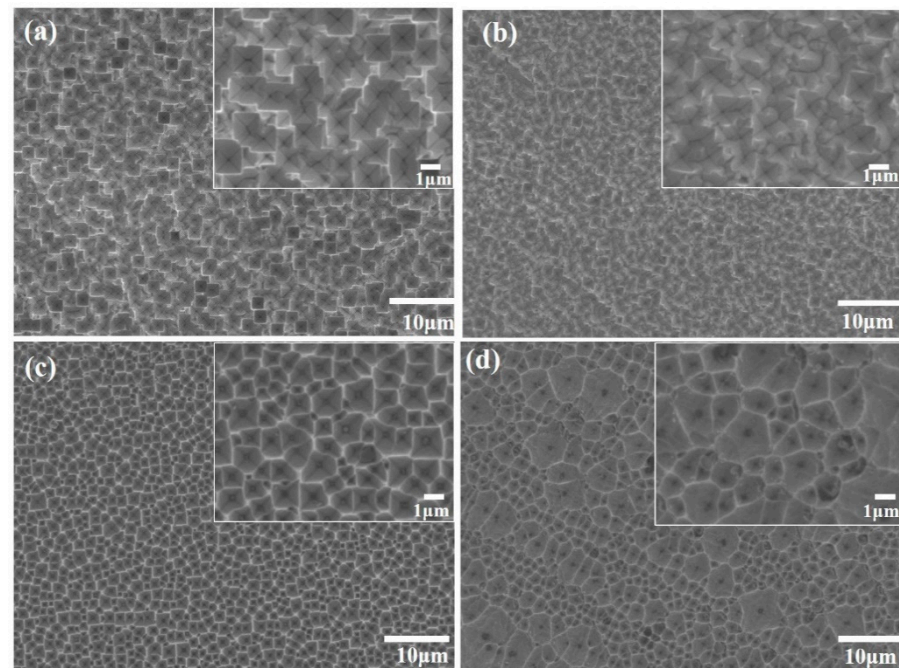


Figure 12. SEM images of uniform inverted pyramid structure fabricated by NSR technology (a) and Ag@PVP-ACE (b) and the morphology transformation with increasing etching time in NSR process (c) and Ag@PVP-ACE process (d).

4.2. Comparative Analysis of the Optical Properties of Upright Pyramid and the Inverted Pyramid

The Si surface reflectivity of the inverted pyramid was significantly lower than that of an upright pyramid, as shown in Figure 13a. As for the randomly distributed upright pyramid (Figure 13b,d), 89% of incident rays suffered a double bounce (path A), and 11% occurred a triple bounce [51] (path B). However, the reflection paths of the randomly distributed inverted pyramid (Figure 13c) increased from two to three, the rays incident on the pyramid at smaller angles (path C) and 42% of incident rays suffered triple bounces [52,53]. The higher reflection frequency effectively reduced the surface reflectivity. Correspondingly, the energy mostly gathered inside the inverted pyramid, which had stronger energy collection efficiency [5].

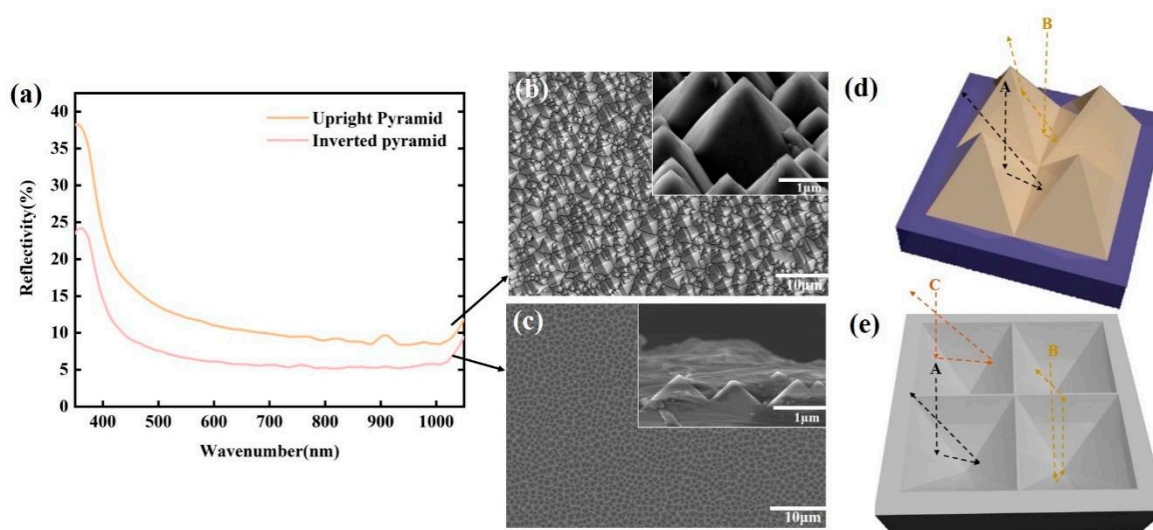


Figure 13. Reflectance spectra (a), SEM images (b,c) and possible reflection paths (d,e) of inverted and upright pyramids.

5. Conclusions

In this paper, an efficient fabrication method for inverted pyramids of Si wafers by silver ion-assisted chemical etching with the synergism of PVP was investigated. The etching behavior with the addition of PVP into Ag–ACE solution exhibited two statuses: polishing or fabricating inverted pyramid. The critical factors for fabricating microstructure were demonstrated. The effect of various experimental parameters on the etching results in Ag@PVP–ACE was verified. Furthermore, we compared the inverted pyramid obtained by NSR technology and Ag@PVP–ACE, and the advantages of Ag@PVP–ACE were analyzed. Consequently, as a simple and low-cost one-step method to fabricate an inverted pyramid, we believe that the Ag@PVP–ACE process is a powerful solution with its simplicity and stability and may have application potential in solar cell, Si photoelectrode sensor, optical element and superhydrophobic surface. In addition, we hope that our work could provide a new strategy for utilizing organic molecules to control the etching behavior of the Ag/Si interface in the MACE solution.

Author Contributions: Y.L.: Conceptualization, investigation, data processing, writing—original draft. K.D.: revision, characterization. L.B.: grammar. Z.G.: formal analysis, funding acquisition, supervision, project administration, writing—review and editing. All authors have read and agreed to the published version of the manuscript.

Funding: This research was funded by the Jiangsu Collaborative Innovation Center for Advanced Inorganic Function Composites, the Priority Academic Program Development of Jiangsu Higher Education Institutions (PAPD).

Data Availability Statement: Not applicable.

Acknowledgments: This work was supported by funding of Jiangsu Collaborative Innovation Center for Advanced Inorganic Function Composites, the Priority Academic Program Development of Jiangsu Higher Education Institutions (PAPD) and Nanjing Naxin New Material Co., Ltd. (Nanjing, Jiangsu, China).

Conflicts of Interest: We would like to declare on behalf of my co-authors that the work described was original research that has not been published previously and not under consideration for publication elsewhere, in whole or in part. All the authors listed have approved the manuscript that is enclosed. No conflict of interest exists in the submission of this manuscript, and the manuscript is approved by all authors for publication.

References

1. Wang, Y.; Yang, L.; Liu, Y.; Mei, Z.; Chen, W.; Li, J.; Liang, H.; Kuznetsov, A.; Xiaolong, D. Maskless inverted pyramid texturization of silicon. *Sci. Rep.* **2015**, *5*, 10843. [[CrossRef](#)] [[PubMed](#)]
2. Liu, Y.; Lai, T.; Li, H.; Wang, Y.; Mei, Z.; Liang, H.; Li, Z.; Zhang, F.; Wang, W.; Kuznetsov, A.Y.; et al. Nanostructure formation and passivation of large-area black silicon for solar cell applications. *Small* **2012**, *8*, 1392–1397. [[CrossRef](#)] [[PubMed](#)]
3. Yang, X.; Zhang, W.; Choi, J.; Ta, H.Q.; Bai, Y.; Chen, L.; Zhang, M.; Chen, Y.; Guan, Z.; Rummeli, M.H.; et al. Influence of bowl-like nanostructures on the efficiency and module power of black silicon solar cells. *Sol. Energy* **2019**, *189*, 67–73. [[CrossRef](#)]
4. Zhang, P.; Jia, R.; Tao, K.; Jiang, S.; Dai, X.; Sun, H.; Jin, Z.; Ji, Z.; Liu, X.; Zhao, C.; et al. The influence of Ag-ion concentration on the performance of mc-Si silicon solar cells textured by metal assisted chemical etching (MACE) method. *Sol. Energy Mater. Sol. Cells* **2019**, *200*, 109983. [[CrossRef](#)]
5. Zhang, C.; Chen, L.; Zhu, Y.; Guan, Z. Fabrication of 20.19% Efficient Single-Crystalline Silicon Solar Cell with Inverted Pyramid Microstructure. *Nanoscale Res. Lett.* **2018**, *13*, 91. [[CrossRef](#)] [[PubMed](#)]
6. Mrazkova, Z.; Sobkowicz, I.P.; Foldyna, M.; Postava, K.; Florea, I.; Pištora, J.; Roca i Cabarrocas, P. Optical properties and performance of pyramidal texture silicon heterojunction solar cells: Key role of vertex angles. *Prog. Photovolt. Res. Appl.* **2018**, *26*, 369–376. [[CrossRef](#)]
7. Han, S.J.; Ghosh, S.; Abudayyeh, O.K.; Hoard, B.R.; Culler, E.C.; Bonilla, J.E.; Han, S.M.; Han, S.E. Symmetry-breaking nanostructures on crystalline silicon for enhanced light trapping in thin film solar cells. *Opt. Express* **2016**, *24*, 1586–1596. [[CrossRef](#)] [[PubMed](#)]
8. Gu, H.; Guan, Z.; Liu, Y. Large-scale preparation of 22.06% efficiency single-crystalline silicon solar cells with inverted pyramid microstructure through nanostructure rebuilding treatment. *Mater. Res. Express* **2020**, *7*, 096203. [[CrossRef](#)]
9. Zhao, J.; Wang, A.; Green, M.A.; Ferrazza, F. 19.8% efficient “honeycomb” textured multicrystalline and 24.4% monocrystalline silicon solar cells. *Appl. Phys. Lett.* **1998**, *73*, 1991–1993. [[CrossRef](#)]
10. Huang, Z.; Geyer, N.; Werner, P.; de Boer, J.; Gosele, U. Metal-assisted chemical etching of silicon: A review. *Adv. Mater.* **2011**, *23*, 285–308. [[CrossRef](#)]
11. Cacciato, A.; Duerinckx, F.; Baert, K.; Moors, M.; Caremans, T.; Leys, G.; De Keersmaecker, K.; Szlufcik, J. Investigating manufacturing options for industrial PERL-type Si solar cells. *Sol. Energy Mater. Sol. Cells* **2013**, *113*, 153–159. [[CrossRef](#)]
12. Koynov, S.; Brandt, M.S.; Stutzmann, M. Black nonreflecting silicon surfaces for solar cells. *Appl. Phys. Lett.* **2006**, *88*, 203107. [[CrossRef](#)]
13. Kan, M.; Yan, Z.W.; Wang, X.; Hitt, J.L.; Xiao, L.; McNeill, J.M.; Wang, Y.; Zhao, Y.; Mallouk, T.E. 2-Aminobenzenethiol-Functionalized Silver-Decorated Nanoporous Silicon Photoelectrodes for Selective CO₂ Reduction. *Angew. Chem. Int. Ed. Engl.* **2020**, *59*, 11462–11469. [[CrossRef](#)]
14. Qin, Y.; Cui, Z.; Wen, Z.; Bai, Y. Highly sensitive NO₂ sensors based on core-shell array of silicon nanowires/polypyrrole and new insight into gas sensing mechanism of organic/inorganic hetero-contact. *Polym. Compos.* **2019**, *40*, 3275–3284. [[CrossRef](#)]
15. Zhang, B.; Wang, H.; Lu, L.; Ai, K.; Zhang, G.; Cheng, X. Large-Area Silver-Coated Silicon Nanowire Arrays for Molecular Sensing Using Surface-Enhanced Raman Spectroscopy. *Adv. Funct. Mater.* **2008**, *18*, 2348–2355. [[CrossRef](#)]
16. Kumar, A.; Dhasmana, H.; Kumar, A.; Kumar, V.; Verma, A.; Jain, V.K. Highly sensitive MWCNTs/SiNWs hybrid nanostructured sensor fabricated on silicon-chip for alcohol vapors detection. *Phys. E Low-Dimens. Syst. Nanostructures* **2020**, *127*, 114538. [[CrossRef](#)]
17. Zhang, M.-L.; Yi, C.-Q.; Fan, X.; Peng, K.-Q.; Wong, N.-B.; Yang, M.-S.; Zhang, R.-Q.; Lee, S.-T. A surface-enhanced Raman spectroscopy substrate for highly sensitive label-free immunoassay. *Appl. Phys. Lett.* **2008**, *92*, 043116. [[CrossRef](#)]
18. Boukai, A.I.; Bunimovich, Y.; Tahir-Kheli, J.; Yu, J.K.; Goddard, W.A.; Heath, J.R. Silicon nanowires as efficient thermoelectric materials. *Nature* **2008**, *451*, 168–171. [[CrossRef](#)] [[PubMed](#)]
19. Hochbaum, A.I.; Chen, R.K.; Delgado, R.D.; Liang, W.J.; Garnett, E.C.; Najarian, M.; Majumdar, A.; Yang, P.D. Enhanced thermoelectric performance of rough silicon nanowires. *Nature* **2008**, *451*, 163–165. [[CrossRef](#)]
20. Cho, S.; Jung, W.; Jung, G.Y.; Eom, K. High-performance boron-doped silicon micron-rod anode fabricated using a mass-producible lithography method for a lithium ion battery. *J. Power Sources* **2020**, *454*, 227931. [[CrossRef](#)]
21. Kim, Y.Y.; Kim, H.J.; Jeong, J.H.; Lee, J.; Choi, J.H.; Jung, J.Y.; Lee, J.H.; Cheng, H.; Lee, K.W.; Choi, D.G. Facile Fabrication of Silicon Nanotube Arrays and Their Application in Lithium-Ion Batteries. *Adv. Eng. Mater.* **2016**, *18*, 1349–1353. [[CrossRef](#)]

22. Magasinski, A.; Dixon, P.; Hertzberg, B.; Kvit, A.; Ayala, J.; Yushin, G. High-performance lithium-ion anodes using a hierarchical bottom-up approach. *Nat. Mater.* **2010**, *9*, 353–358. [[CrossRef](#)]
23. Song, Y.; Mohseni, P.K.; Kim, S.H.; Shin, J.C.; Ishihara, T.; Adesida, I.; Li, X. Ultra-High Aspect Ratio InP Junctionless FinFETs by a Novel Wet Etching Method. *IEEE Electron. Device Lett.* **2016**, *37*, 970–973. [[CrossRef](#)]
24. Van Toan, N.; Toda, M.; Ono, T. High Aspect Ratio Silicon Structures Produced via Metal-Assisted Chemical Etching and Assembly Technology for Cantilever Fabrication. *IEEE Trans. Nanotechnol.* **2017**, *16*, 567–573. [[CrossRef](#)]
25. Van Toan, N.; Wang, X.Y.; Inomata, N.; Toda, M.; Voiculescu, I.; Ono, T. Low Cost and High-Aspect Ratio Micro/Nano Device Fabrication by Using Innovative Metal-Assisted Chemical Etching Method. *Adv. Eng. Mater.* **2019**, *21*, 9. [[CrossRef](#)]
26. Owen, J.; Hildreth, W.L.; Ching Ping, W. Effect of Catalyst Shape and Etchant Composition on Etching Direction in Metal-Assisted Chemical Etching of Silicon to Fabricate 3D Nanostructures. *ACS Nano* **2009**, *3*, 10.
27. Lai, R.A.; Hymel, T.M.; Narasimhan, V.K.; Cui, Y. Schottky Barrier Catalysis Mechanism in Metal-Assisted Chemical Etching of Silicon. *ACS Appl. Mater. Interfaces* **2016**, *8*, 8875–8879. [[CrossRef](#)]
28. Wu, Y.; Gao, F.; Wu, H.; Liu, X.; Zheng, X.; Liu, S.; Wang, H.; Zhou, S.; Li, F. Motility of Metal Nanoparticles in Silicon and Induced Anisotropic Silicon Etching. *Adv. Funct. Mater.* **2008**, *18*, 3026–3035.
29. Wu, Y.; Gao, F.; Wu, H.; Liu, X.; Zheng, X.; Liu, S.; Wang, H.; Zhou, S.; Li, F. The effects of Ag particle morphology on the antireflective properties of silicon textured using Ag-assisted chemical etching. *J. Alloy. Compd.* **2016**, *670*, 156–160. [[CrossRef](#)]
30. Pinna, E.; Le Gall, S.; Torralba, E.; Mula, G.; Cachet-Vivier, C.; Bastide, S. Mesopore Formation and Silicon Surface Nanostructure by Metal-Assisted Chemical Etching With Silver Nanoparticles. *Front. Chem.* **2020**, *8*, 658. [[CrossRef](#)]
31. Omer, A.-A.-A.; Yang, Y.; Sheng, G.; Li, S.; Yu, J.; Ma, W.; Qiu, J.; Kolaly, W.E. Nano-Texturing of Silicon Wafers Via One-Step Copper-Assisted Chemical Etching. *Silicon* **2019**, *12*, 231–238. [[CrossRef](#)]
32. Huang, J.C.; Sen, R.K.; Yeager, E. Oxygen Reduction on Platinum in 85% Orthophosphoric Acid. *J. Electrochem. Soc.* **2019**, *12*, 786–792. [[CrossRef](#)]
33. Xiaohua Cai, K.K.; Gottjiried, K.; Christian, N.; Wolfgang, D.; Ogorevc, B. Electrocatalytic Reduction of Hydrogen Peroxide on a PalladiumModified Carbon Paste Electrode. *Electroanalysis* **1995**, *4*, 340–345.
34. Zeis, R.; Lei, T.; Sieradzki, K.; Snyder, J.; Erlebacher, J. Catalytic reduction of oxygen and hydrogen peroxide by nanoporous gold. *J. Catal.* **2008**, *253*, 132–138. [[CrossRef](#)]
35. Hu, Y.; Fu, H.; Wang, J.; Sun, R.; Wu, L.; Liu, Y.; Xu, J.; Liu, J.; Peng, K.-Q. Carbon induced galvanic etching of silicon in aerated HF/H₂O vapor. *Corros. Sci.* **2019**, *157*, 268–273. [[CrossRef](#)]
36. Wang, J.; Hu, Y.; Zhao, H.; Fu, H.; Wang, Y.; Huo, C.; Peng, K.Q. Oxidant Concentration Modulated Metal/Silicon Interface Electrical Field Mediates Metal-Assisted Chemical Etching of Silicon. *Adv. Mater. Interfaces* **2018**, *5*, 1801132. [[CrossRef](#)]
37. Yang, W.; Shen, H.; Jiang, Y.; Tang, Q.; Raza, A.; Gao, K. Formation of Inverted Pyramid-Like Submicron Structures on Multicrystalline Silicon Using Nitric Acid as Oxidant in Metal Assisted Chemical Etching Process. *Phys. Status Solidi A* **2019**, *216*, 1800636. [[CrossRef](#)]
38. Kolasinski, K.W.; Barclay, W.B. The stoichiometry of electroless silicon etching in solutions of V₂O₅ and HF. *Angew. Chem. Int. Ed. Engl.* **2013**, *52*, 6731–6734. [[CrossRef](#)]
39. Choi, J.-Y.; Honsberg, C. Sub-Wavelength Scale Si Inverted Pyramid Fabrication with Enhanced Size Control by Using Silica Sphere Lithography Technique. *Appl. Sci.* **2018**, *8*, 1720. [[CrossRef](#)]
40. Zhao, Y.; Liu, Y.; Chen, W.; Wu, J.; Chen, Q.; Tang, H.; Wang, Y.; Du, X. Regulation of surface texturization through copper-assisted chemical etching for silicon solar cells. *Solar Energy* **2020**, *201*, 461–468. [[CrossRef](#)]
41. Wu, J.; Liu, Y.; Chen, Q.; Chen, W.; Yang, L.; Wang, Y.; He, M.; Du, X. The orientation and optical properties of inverted-pyramid-like structures on multi-crystalline silicon textured by Cu-assisted chemical etching. *Solar Energy* **2018**, *171*, 675–680. [[CrossRef](#)]
42. Wu, J.; Liu, Y.; Chen, W.; Zhao, Y.; Chen, Q.; Tang, H.; Wang, Y.; Du, X. Influence of different-sized inverted-pyramids of silicon texture by Ag manipulation on solar cell performance. *Appl. Surf. Sci.* **2020**, *506*, 144778. [[CrossRef](#)]
43. Tang, Q.; Shen, H.; Yao, H.; Gao, K.; Ge, J.; Liu, Y. Investigation of optical and mechanical performance of inverted pyramid based ultrathin flexible c-Si solar cell for potential application on curved surface. *Appl. Surf. Sci.* **2020**, *504*, 144588. [[CrossRef](#)]
44. Brahiti, N.; Bouanik, S.-A.; Hadjersi, T. Metal-assisted electroless etching of silicon in aqueous NH₄HF₂ solution. *Appl. Surf. Sci.* **2012**, *258*, 5628–5637. [[CrossRef](#)]
45. Koker, L.; Kolasinski, K.W. Laser-Assisted Formation of Porous Si in Diverse Fluoride Solutions: Reaction Kinetics and Mechanistic Implications. *ACS J. Phys. Chem. B* **2001**, *8*, 3864–3871. [[CrossRef](#)]
46. Qi, X.; Balankura, T.; Zhou, Y.; Fichthorn, K.A. How Structure-Directing Agents Control Nanocrystal Shape: Polyvinylpyrrolidone-Mediated Growth of Ag Nanocubes. *Nano Lett.* **2015**, *15*, 7711–7717. [[CrossRef](#)]
47. Zhang, X.; Liu, B.; Hu, C.; Chen, S.; Liu, X.; Liu, J.; Chen, F.; Chen, J.; Xie, F. A facile method in removal of PVP ligands from silver nanowires for high performance and reusable SERS substrate. *Spectrochim. Acta A Mol. Biomol. Spectrosc.* **2020**, *228*, 117733. [[CrossRef](#)]
48. Mao, H.; Feng, J.; Ma, X.; Wu, C.; Zhao, X. One-dimensional silver nanowires synthesized by self-seeding polyol process. *J. Nanoparticle Res.* **2012**, *14*, 1–5. [[CrossRef](#)]

49. Abramova, E.N.; Khort, A.M.; Gvelesiani, A.A.; Yakovenko, A.G.; Shvets, V.I. A model of the mechanism of the chemical interaction of the etchant ion (HF₂)⁻ with silicon during its electrochemical etching in hydrofluoric acid solutions. *Dokl. Chem.* **2016**, *470*, 252–254. [[CrossRef](#)]
50. Lee, J.; Wong, C.C.D.; Tung, C.Y.; Smith, W.L.; Hahn, S.; Arst, M. Gate oxide integrity and minority-carrier lifetime correlated with Si wafer polish damage. *Appl. Phys. Lett.* **1987**, *51*, 54–56. [[CrossRef](#)]
51. Baker-Finch, S.C.; McIntosh, K.R. Reflection distributions of textured monocrystalline silicon: Implications for silicon solar cells. *Prog. Photovolt. Res. Appl.* **2012**. [[CrossRef](#)]
52. Baker-Finch, S.C.; McIntosh, K.R. Reflection of normally incident light from silicon solar cells with pyramidal texture. *Prog. Photovolt. Res. Appl.* **2011**, *19*, 406–416. [[CrossRef](#)]
53. Chen, Q.; Liu, Y.; Wang, Y.; Chen, W.; Wu, J.; Zhao, Y.; Du, X. Optical properties of a random inverted pyramid textured silicon surface studied by the ray tracing method. *Solar Energy* **2019**, *186*, 392–397. [[CrossRef](#)]